DIFFUSION OF A PLASMA SUBJECT TO NEUTRAL BEAM INJECTION

H. Okuda and S. Hiroe*

Plasma Physics Laboratory, Princeton University

Princeton, NJ 08544

PPPL--2388

DE87 003076

ABSTRACT

Two-dimensional numerical plasma simulations have been carried out in a uniform magnetic field to study the effects of neutral beam injection on plasma diffusion. Neutral beams injected across a magnetic field are assumed to be ionized by various ionization processes in a plasma. It is found that the suprathermal convective motion of a plasma generated by the injection of neutral beams is dissipated via anomalous viscosity, leading to enhanced cross-field diffusion. The diffusion coefficient depends weakly on the magnetic field and plasma density, similar to the diffusion due to thermally excited convective cells. The magnitude of the diffusion increases with the injection energy and is much larger than the thermal diffusion because of the presence of suprathermal plasma convection. It is shown that a similar anomalous plasma diffusion may occur in a plasma subject to radio frequency (RF) wave heating where only a localized region of plasma across a magnetic field is heated to a temperature much higher than the surrounding temperature. Theoretical investigations are given on the scaling of enhanced plasma diffusion.

*Permanent address: Oak Ridge National Laboratory, Oak Ridge, TN 37831

I. INTRODUCTION

Injection of fast neutral beams into a confined plasma in a magnetic field has proved to be an attractive and efficient means for heating laboratory plasmas to thermonuclear temperatures.[1-3] Neutral beams injected into an ambient plasma are ionized by electron and ion collisions and charge exchange so that the resultant high energy ions are trapped in a magnetic field. For the case of neutral beam injection into a toroidal plasma, trajectories of fast ions in a magnetic field have been studied.[4] It has been found that the drift orbits of high energy ions can be quite large for the case of perpendicular injection as well as counter injection in which the neutral beams are injected along the toroidal magnetic field but antiparallel to the direction of current flow. Heating of the ambient plasma via neutral beam injection is attained as the injected beam particles undergo collisions with the plasma ions and electrons. Energy variation of the injected ions as well as the slowing-down time of the injected ions to the thermal energy have been calculated in detail.[4]

These calculations on the trajectories of injected ions and collisions reveal much of the fundamental behavior of injected beams. However, they do not address the collective effects of neutral beam injection on plasma confinement. As the injected particles are ionized, an electric field $\underline{E} = -\underline{V} \times \underline{B}/c$ is induced through polarization of the plasma, which convects both the beam and the ambient plasma in the direction of injection. $\underline{V}$ is the velocity of plasma flow across the magnetic field. Such a convective motion across the magnetic field can be dissipated by anomalous viscosity, leading to enhanced plasma diffusion.

In this paper we shall study basic properties of plasma diffusion associated with perpendicular neutral beam injection in a slab geometry with a

uniform magnetic field. Extensions to more realistic geometries will be considered in future communications.[5]

In Sec. II, the simulation model in the presence of neutral beam injection is introduced and the results of simulations are given. The effects of localized plasma heating via radio frequency waves on plasma diffusion are considered in Sec. III. Discussion and theoretical studies of simulation results are given in Sec. IV.

II. NEUTRAL BEAM INJECTION AND PLASMA DIFFUSION

Let us consider a two-dimensional plasma model immersed in a uniform magnetic field as shown in Fig. 1. The magnetic field is assumed to be perpendicular to the x-y plane of the simulations. Neutral beams are assumed to be injected across the magnetic field at a velocity of $\underline{V} = V_o \hat{x}$ over a distance of δ in y. As the injected beams are ionized, an electric field is induced in a plasma which generates plasma convection across the magnetic field via $c\underline{E} \times \underline{B}/B^2$ drift. Such an electric field can be regarded as a result of plasma polarization at the edges of the finite-size neutral beams as shown in Fig. 1. As the beam particles drift across the ambient plasma, a shear flow is generated which is dissipated via anomalous viscosity, thus leading to an enhanced cross-field plasma diffusion due to neutral beam injection.

Two-dimensional numerical simulations are carried out using the geometry and initial conditions shown in Fig. 1. The ambient plasma is initially uniform in the two-dimensional (x, y) planes perpendicular to a magnetic field. Neutral beams injected from the left over a distance of δ in the y-direction at a velocity of $\underline{V}_o = V_o \hat{x}$ are assumed to be ionized at $t = 0$. Beam ions and electrons are assumed to be on top of each other at $t = 0$ which models the injection of neutral particles and subsequent ionization. Since

the simulated plasma represents only a small portion of an infinite plasma, periodic boundary conditions are used. Typical simulation parameters are: 64 x 64 two-dimensional grids, the ambient electron and ion Debye length $\lambda_e = \lambda_i = \Delta$ where Δ is the grid size, 4 - 16 simulation particles per grid for the ambient particles, mass ratio $m_i/m_e = 2$, and the ratio of the electron gyrofrequency to the electron plasma frequency, $\omega_{ce}/\omega_{pe} = 1, 2, 4$. Since the plasma motion is governed by the $c\underline{E} \times \underline{B}/B^2$ in a two-dimensional model, use of a small mass ratio does not modify the diffusion in any significant way and serves to reduce computing time while allowing us to follow the exact dynamics of the system.[6] The initial beam density is uniform both in x and y but is localized in y over a distance δ as shown in Fig. 1. The initial velocity distributions for the ambient particles are the thermal Maxwellians while the beam particles are injected at the velocity $V_o\hat{x}$ superimposed on the thermal distribution whose temperature is equal to the ambient plasma temperature. The injection energy is taken to be much larger than the plasma temperature. This initial distribution is assumed to model the neutral beam injection and the subsequent ionization. As the beam particles gyrate around the magnetic field, a polarization electric field is set up which causes the particles to drift due to $c\underline{E} \times \underline{B}/B^2$ drift as shown in Fig. 1. Such a convective motion is rapidly dissipated in a plasma via anomalous viscosity, leading to enhanced diffusion.

In order to obtain an insight into the enhanced diffusion, we shall first study a simulation of a uniform thermal Maxwellian plasma without beam particles (case 1) and compare the result with the results in the presence of beam particles. Figure 2 shows the positions of the selected particles (ions) in the (x, y) plane at four different instances of time. These particles are initially located in a narrow strip of a width δ in y and uniform in x. n_o =

$4/\Delta^2$ and $\omega_{ce} = \omega_{pe}$ is chosen where n_o is the number density of the ambient particles per grid. As shown in Fig. 2, the particles slowly spread out in space which leads to enhanced plasma diffusion due to thermally excited convective cells. The diffusion coefficient in the y-direction, D_y, may be determined from the measurement of $\langle(\Delta y)^2\rangle$ for a set of particles where Δy is the displacement of a particle location between $t = 0$ and $t = t$. D_y is then defined by

$$D_y = \frac{\langle(\Delta y)^2\rangle}{2t} \quad , \tag{1}$$

where $\langle \quad \rangle$ means averaging over many particles.

Figure 3 shows the measured $\langle(\Delta y)^2\rangle$, which exemplifies the characteristic behavior of the diffusion process. For a time shorter than the correlation time, $\langle(\Delta y)^2\rangle$ is proportional to t^2, which represents a drift motion. But for a time longer than the correlation time. $\langle(\Delta y)^2\rangle$ is proportional to like t resulting in the diffusion process. The measured diffusion coefficient is $D_y = 0.044\ \Delta^2\omega_{pe}$ which is close to that predicted from the diffusion of thermally excited convective cells given by[6]

$$D_x = D_y = \frac{c}{2B}\left[\frac{T}{1 + \omega_{pi}^2/\omega_{ci}^2 + \omega_{pe}^2/\omega_{ce}^2}\right]^{1/2}\left(\ln \frac{k_{max}L}{2\pi}\right)^{1/2} \quad , \tag{2}$$

where ω_{pi} and ω_{ci} are ion plasma frequency and ion gyrofrequency, L is the system size, and k_{max} is the maximum wave number of the electric field. Note Eq. (2) is smaller than Eq. (1a) of Ref. 6 because of the difference in the definition of the diffusion coefficient. Diffusion in the x-direction is more or less the same as that shown in Fig. 3, indicating that the diffusion process is isotropic in the x-y plane.

Figure 4 shows the instantaneous contour plots of the electrostatic potential, $e\phi/T$, at $\omega_{pe}t$ = 50 and 500. It is clear that the potential structure is dominated by small scale contours. This contrasts sharply with plasmas that are subject to neutral beam injection. Note also that the amplitude of the potential is large even in thermal equilibrium. This is because the convective cells satisfy $e\phi/T \gg \delta n/n$ in contrast to drift waves which satisfy $e\phi/T \sim \delta n/n$, where δn is the density perturbation.[7]

In the presence of neutral beam injection, plasma diffusion along and across the direction of beam injection is not necessarily the same, so it is more convenient to measure D_x and D_y separately. We should emphasize that the simulation results shown in Fig. 2 demonstrate a presence of anomalous diffusion via plasma convection even in thermal equilibrium.

We shall now study a case where a plasma is subject to neutral beam injection so that a large amplitude suprathermal plasma convection is generated. The first such example (case 2) corresponds to a low density, neutral beam injection in which the beam density is a quarter of the background density, $n_b = n_o/4$. Note that the beam particles are localized in the y-direction with its width $\delta = L_y/4 = 16\ \Delta$ so that the beam density averaged over the entire two-dimensional plane is only 1/16 of the ambient density. $n_o = 4/\Delta^2$, $\omega_{ce} = 2\ \omega_{pe}$, and $V_o/V_i = 5$ are chosen, giving the initial beam ion gyroradius $\rho_b/\Delta = 5/\sqrt{2}$. Here V_i is the ion thermal speed.

Figure 5 shows the positions of the ambient, (a), (b), and the beam (c), (d), ions at $\omega_{pe}t$ = 250 and 500. For both the beam and the ambient ions, a vortex structure develops leading to a rapid plasma diffusion that dissipates the density gradient in the y-direction. Note that the total plasma density is larger at the center of a plasma where the beam particles are located initially. This is discussed later.

It is interesting to observe that $\langle(\Delta x)^2\rangle$ and $\langle(\Delta y)^2\rangle$ behave quite differently in the presence of neutral beam injection as indicated in Fig. 6. Displacement perpendicular to the beam injection, $\langle(\Delta y)^2\rangle$, increases as t^2 for a while and then as t. This gives rise to a diffusion coefficient $D_y = 1.5\ \Delta^2\omega_{pe}$ which is much larger than the corresponding diffusion in a thermal plasma as shown in Fig. 3. Note $\langle(\Delta y)^2\rangle$ shown in Fig. 6 is for the ambient ions, but it is about the same as that for the beam ions as shown in Fig. 5. Displacement $\langle(\Delta x)^2\rangle$ in the direction of beam injection behaves quite differently from $\langle(\Delta y)^2\rangle$. $\langle(\Delta x)^2\rangle$ shown in Fig. 6 is for the beam ions. Beam ion drift velocity V_x associated with neutral beam injection after ionization can be determined from $\langle(\Delta x)^2\rangle = V_x^2 t^2$, giving rise to $V_x/V_i = 0.27$, which is much smaller than the initial neutral beam velocity $V_o/V_i = 5$. This suggests that the large part of injection velocity is kept in the gyromotion. This convection in x is apparently caused by the cE_y/B drift associated with the polarization electric field generated by the charges at the edges of the beam. This convection is rapidly dissipated and $\langle(\Delta x)^2\rangle$ goes like t for large t as shown in Fig. 6, giving $D_x = 1.7\ \Delta^2\omega_{pe}$. It is interesting to note that D_x is comparable to $D_y = 1.5\ \Delta^2\omega_{pe}$ at the late stage of simulation where the convective motion has reached a steady state. At this final stage of $\langle(\Delta x)^2\rangle$, it is clear that suprathermal plasma convection has mixed the beam and ambient plasma more or less equally, which dissipates the initial anisotropic plasma convection associated with the beam injection.

Comparing the two diffusion coefficients for case 1 and case 2, we may define the effective temperature T_{eff} of the plasma subject to neutral beam injection relative to the thermal plasma from Eq. (2), finding

$$\frac{T_{eff}}{T} = (1.5/0.044)^2 = 1160 \quad .$$

This suggests that the energy in the convective plasma motion in the presence of neutral beam injection is three orders of magnitude larger than the energy in thermal convection. Note in a real plasma where the thermal diffusion is much smaller than the simulation plasma, the enhancement factor of diffusion in the presence of neutral beam injection over thermal diffusion can be much greater.

It should be emphasized that the diffusion discussed here actually dissipates the initial density gradients which are generated as a result of neutral beam injection. Figure 7 shows the instantaneous ion density in the y direction averaged over the x direction at $t = 0$ and $\omega_{pe}t = 950$. The initial square density jump at the center of the plasma is completely diffused out at the end of the simulation. Note that the relatively large density fluctuations persist, indicating that the plasma motion is dominated by the suprathermal convective cells.

Rapid diffusion in the ion velocity space also takes place as shown in Fig. 8 which is the instantaneous total ion velocity distribution in v_x integrated over v_y, $f(v_x) = \int f(v_x, v_y)dv_y$ at $\omega_{pe}t = 5$ and 500. It is clear that the high energy beam ions are rapidly thermalized and the total velocity distribution appears to approach that of a thermal plasma. What happened is that the initial ion beam distribution is unstable with respect to the high frequency loss-cone instability near the ion gyroharmonic waves, which causes a rapid diffusion in velocity space.[8] Measurements of the frequency spectrum reveal the presence of large amplitude waves whose frequencies are near the ion gyroharmonics, confirming such velocity space instability. This is discussed later.

Figure 9 shows the time history of the average ion energy per particle for the ambient and the beam ions. It is clear that the average beam ion energy remains much larger than the average ambient ion energy. The initial rapid relaxation is caused by the generation of the polarization electric field at the edges of the beam ions, which accelerated some of the ambient ions to higher energy. High frequency waves near the ion gyroharmonic frequencies also contributed to the heating of the ambient ions. As will be shown later, the high frequency electrostatic instability contributes little to particle cross-field diffusion because of the high frequency $\omega \gtrsim \omega_{ci}$, and short wavelength, $\lambda \gtrsim \rho_i$, nature of the instability. Measurements of the frequency spectrum of the electric field reveal a presence of high frequency ion gyroharmonic waves in addition to a low frequency peak near $\omega \approx 0$, which corresponds to turbulent plasma convection.

When the beam density is increased to equal the ambient density in the region of neutral beam injection, $n_b = n_o$, while keeping all the other parameters the same, we found the results shown in Fig. 10 (case 3). The measurements of $\langle(\Delta x)^2\rangle$ reveal that the initial beam convection velocity is now much larger, $V_x/V_i \approx 0.88$. The convection velocity is still much smaller than the neutral beam injection velocity $V_o/V_i = 5$. The diffusion coefficient across the beam injection is increased by a factor of 2 compared to case 2, giving rise to $D_y = 2.8\ \Delta^2\omega_{pe}$, which suggests that the diffusion coefficient scales as the square root of the injection energy $D \sim (T_{eff})^{1/2}$.

Figure 11 shows the instantaneous contour plots of the electrostatic potential for case 3 at $\omega_{pe}t = 25$, 125, 250, and 500. Note the initial laminar contours aligned along the direction of the beam injection become more and more isotropic and at the same time coalesce into larger scale contours. At $\omega_{pe}t = 500$, the size of the contour is as large as the system size, which

persists over the course of the simulation. Note the amplitude of the potential contours is much larger here than for the thermal plasma shown in Fig. 3 and is close to the neutral beam injection energy, $e\phi/m_{io}^2 \sim 1$.

When the beam density is further increased to $n_b = 2.25\ n_o$ while keeping all the other simulation parameters the same as in case 3, we found $D_x = 4.8\ \Delta^2\omega_{pe}$ and $D_y = 4.5\ \Delta^2\omega_{pe}$ in steady state. The convection velocity in the x direction is found to be $V_x/V_i = 1.3$.

It is interesting to study the dependence of D_y on B. This was done by using the same parameters as in case 3 but changing $\omega_{ce}/\omega_{pe} = 1$, 2, and 4. The results are shown in Fig. 12 for D_y. We found that the diffusion coefficient D_y does not change much for $\omega_{ce}/\omega_{pe} = 1$ and 2 but for $\omega_{ce}/\omega_{pe} = 4$, D_y is smaller by a factor of 2 indicating $D_y \sim B^{-1}$ dependence in a strong magnetic field, $\omega_{pi}^2/\omega_{ci}^2 < 1$. This dependence of D_y on B and T_{eff} is consistent with convective diffusion due to thermally excited vortices, but the magnitude of D_y is many orders of magnitude larger due to the suprathermal convection associated with neutral beam injection.

When the injection energy of the neutral beam is reduced, plasma diffusion is also found to decrease (case 4). Figure 13 shows the results of a simulation using $n_b = n_o$, $\omega_{ce}/\omega_{pe} = 2$, and $V_o/V_i = 2.5$ so that the injection speed is reduced by a factor of 2 from that of case 3. The diffusion coefficient is found to be $D_y = 1.0\ \Delta^2\omega_{pe}$, which should be compared with $D_y = 2.8\ \Delta^2\omega_{pe}$ for case 3. Note the initial convection speed in the x-direction $V_x/V_i = 0.49$ is about a factor of 2 smaller than that of case 3. The final steady-state diffusion coefficient in x is $D_x = 1.2\ \Delta^2\omega_{pe}$ which is about the same as D_y, confirming that the initial anisotropic convection relaxed to the homogeneous vortex flow.

We then examined the dependence of plasma diffusion on the ambient density while fixing the neutral beam density. The parameters of the simulation are the same as in case 3 except for the ambient density which is increased by a factor of 4 so that $n_o = 16/\Delta^2 = 4\ n_b$. $\omega_{ce} = 2\ \omega_{pe}$ and $V_o/V_i = 5$ are used. The results of the simulation show the diffusion coefficient $D_y = 1.2\Delta^2\omega_{pe}$ which is about one-half of $D_y = 2.3\Delta^2\omega_{pe}$ in case 3. This suggests that the enhanced diffusion coefficient scales as $D \sim n_o^{1/2}$ which is similar to the diffusion due to thermal convective cells.[6]

III. RF HEATING AND PLASMA DIFFUSION

In the previous section, we have seen that the convection of a plasma generated as a result of neutral beam injection is dissipated via anomalous viscosity, thus leading to enhanced cross-field diffusion. At the edges of a neutral beam, net charges appear as a result of polarization generating an electric field which drives the plasma convective motion via $c\underline{E} \times \underline{B}/B^2$ drift. When a plasma is subject to localized RF heating such as electron cyclotron or ion cyclotron heating, it is possible that only a small localized region of a plasma attains high temperature relative to the surrounding temperature. Such a high temperature region will spread in space via heat conduction, which could be anomalously fast.

In order to model such a process, a model similar to the model described in Fig. 1 is used. Instead of having beam particles localized in y with its width $\delta = L_y/4$, ambient ions located in that region are assumed hotter than the surrounding particles. Here we do not ask how such particles are heated, but are rather interested in the effects of such local heating on plasma confinement. Since the high energy ions at the localized heating region have larger gyroradii, net charges appear at the boundary of hot and cold plasmas

thereby creating a $c\underline{E} \times \underline{B}/B^2$ convection similar to a plasma subject to the neutral beam injection.

Figure 14 represents results of a simulation using $\omega_{ce} = \omega_{pe}$, $n_o = 4/\Delta^2$, and $T_h = 25\ T_c$ where T_c and T_h are the temperature of the cold plasma and hot ions (case 5). The diffusion in the x- and y-directions behaves similar to a plasma subject to neutral beam injection. $\langle(\Delta x)^2\rangle$ first increases as t^2 indicating a convection due to $c\underline{E} \times \underline{B}/B^2$ drift, reaching $D_x = 2.0\Delta^2\omega_{pe}$. Note the diffusion coefficients observed here are much larger than the thermal diffusion coefficient and are close to the plasma diffusion subject to neutral beam injection.

It is interesting to compare plasma diffusion when the heating is more or less uniform across the magnetic field, such as heating due to alpha particles. Figure 15 shows the result of a simulation in which the hot ions are uniformly spread out across the entire plasma cross section with a Maxwellian velocity distribution (case 6). The parameters of the simulation are $\omega_{ce} = \omega_{pe}$, $n_h = n_o/4$ and $T_h/T_c = 25$. These parameters are the same as that in case 5 except for the uniform initial loading of the hot ions. Both the cold and hot ion diffusion coefficients are plotted. Note that the plasma is isotropic in the x-y plane in this case and no appreciable difference has been observed between D_x and D_y. Diffusion of the cold ambient plasma is $D_c = 0.14\Delta^2\omega_{pe}$ while the hot ions have a smaller diffusion coefficient, $D_h = 0.062\Delta^2\omega_{pe}$. This difference is apparently due to the large gyroradii of the hot ions, $\rho_h = 5\sqrt{2}\Delta$. The cold ion gyroradius is $\rho_c = \sqrt{2}\Delta$. The diffusion of the cold plasma should be compared with the thermal diffusion $D_y = 0.044\Delta^2\omega_{pe}$ as shown in Fig. 3 (case 1). Since the kinetic energy of the hot ions is larger than the cold plasma thermal energy, the diffusion of particles is determined from the hot ion temperature in Eq. (2) suggesting $D \sim T_h^{1/2}$, which is in good agreement with the observed diffusion coefficients in Fig. 15.

Instead of using a thermal Maxwellian velocity distribution for the high energy ions, use of monoenergetic ions, $f(v_\perp) = n_h\delta(v_\perp - V_o)$ may be more appropriate for modeling alpha particle generation. Using the same simulation parameters as in case 6 but using the uniformly distributed hot monoenergetic ions (case 7), we find that the observed diffusion is similar to that shown in Fig. 15. The diffusion, however, is actually smaller by almost a factor of 2, confirming that the high frequency loss-cone instability near the ion gyroharmonics does not cause an enhanced diffusion. Figure 16 shows the ion velocity distributions at $\omega_{pe}t = 0$ and 500. The frequency spectrum of the (1, 1) mode of the electric field is shown in Fig. 17. It is clear that the rapid thermalization of the hot ions is associated with the loss-cone instability.[8] In addition to the peaks near $\omega = \pm 3\ \omega_{ci}$ in the frequency spectrum which are associated with the loss-cone instability, a smaller peak near $\omega = 0$ is clearly seen corresponding to turbulent plasma convective motion.

IV. DISCUSSION

We have shown by means of two-dimensional plasma simulations in a uniform magnetic field that an enhanced cross-field diffusion takes place in a plasma subject to neutral beam injection. Injection of neutral beams and their subsequent ionization generates large-scale plasma convection via $c\underline{E} \times \underline{B}/B^2$ drift where $\underline{E}$ is the electric field associated with the plasma polarization at the edges of the neutral beam. The observed diffusion scales just like the diffusion due to thermally excited convective cells indicating weak dependence on B, n, and T. The diffusion increases with the injection energy. The magnitude of the diffusion is much larger than the thermal convective

diffusion owing to the suprathermal convection generated by the neutral beam injection. Similar large-scale convection and the enhanced diffusion have been studied in detail in a toroidal octupole in which a gun-injected plasma was utilized.[9-11] Drift wave turbulence is also known to excite suprathermal convective cells.[12]

Let us consider a plasma model subject to neutral beam injection as sketched in Fig. 1. As the neutral beams are ionized via various ionization processes, beam ions are trapped by the ambient magnetic field causing the polarization of the beam particles at the edges of the beam. The electric field generated by the polarization in turn causes the beam and plasma to drift via $\underline{V} = c\underline{E} \times \underline{B}/B^2$ across the magnetic field. The resultant drift velocity $\underline{V}$ is found to be much smaller than the injection speed V_o of the neutral beams as measured in our simulations shown in Figs. 6. 10, and 13. The injected beam kinetic energy is shared between the gyromotion of the beam particles after ionization and the convective motion across magnetic field.

The energy density associated with the plasma convection can be given by

$$W = \frac{E^2}{8\pi} + \frac{n_b}{2}(m_e + m_i)\frac{c^2E^2}{B^2} + \frac{n_o}{2}(m_e + m_i)\frac{c^2E^2}{B^2}$$
$$= \frac{E^2}{8\pi}\left[1 + \left(\frac{\omega_{pi}^2}{\omega_{ci}^2} + \frac{\omega_{pe}^2}{\omega_{ce}^2}\right)\left(1 + \frac{n_b}{n_o}\right)\right] , \qquad (3)$$

where the electric field energy, guiding center drift energy of the ambient plasma and the beam plasma are considered. The initial injection energy is given by

$$W_o = \frac{1}{2} n_b (m_i + m_e) V_o^2 , \qquad (4)$$

which is generally much larger than W as shown in our simulations. The major part of the initial injection energy is kept in the gyromotion of the beam particles.

If we assume that a fraction of the initial injection energy is converted to the convection energy of a plasma, $W = \alpha W_o$, then we find

$$\frac{E^2}{8\pi} = \frac{\alpha}{2} \frac{n_b (m_i + m_e) V_o^2}{1 + (\omega_{pi}^2/\omega_{ci}^2 + \omega_{pe}^2/\omega_{ce}^2)(1 + n_b/n_o)} , \qquad (5)$$

which is compared to the thermal distribution per k given by[6]

$$L^2 \frac{E_k^2}{8\pi} = \frac{T}{2} \frac{1}{1+\omega_{pi}^2/\omega_{ci}^2 + \omega_{pe}^2/\omega_{ce}^2} .$$

Assuming the electric field energy is shared equally among different k's as in the thermal plasma, it is straightforward to show that the diffusion coefficient in a plasma with neutral beam injection is modified from Eq. (2) to

$$D_x = D_y = \frac{c}{2B} \left[\frac{T_{eff}}{1 + (\omega_{pi}^2/\omega_{ci}^2 + \omega_{pe}^2/\omega_{ce}^2)(1 + n_b/n_o)}\right]^{1/2} \left(\ln \frac{k_{max} L}{2\pi}\right)^{1/2} \qquad (6)$$

which agrees well with the simulation results reported here. Note that $T_{eff} = \alpha (m_e + m_i) n_b V_o^2/k_{max}^2$ so that the diffusion becomes independent of n_b for $n_b >> n_o$.

In the presence of a density gradient across a magnetic field, one of the authors has shown[13] that the linear dielectric constant for a two-dimensional mode ($k_\parallel = 0$) is given by, for $\omega << \omega_{ci}$,

$$\varepsilon (k, \omega) = 1 + \frac{\omega_{pi}^2}{\omega_{ci}^2} \frac{\omega + i k^2 D}{\omega} \frac{\omega - \omega^*_n}{\omega} , \qquad (7)$$

where

$$\omega^*_n = \frac{kTc}{eB}\frac{\partial \ln n}{\partial x} \tag{8}$$

is the ion diamagnetic drift frequency. The dispersion relation can be obtained from $\varepsilon = 0$ and is found to be

$$\omega = \frac{\omega^*_n}{1 + \omega_{ci}^2/\omega_{pi}^2} + \frac{ik^2D}{1 + \omega_{ci}^2/\omega_{pi}^2} \tag{9}$$

or

$$\omega = -\frac{ik^2D}{1 + \omega_{ci}^2/\omega_{pi}^2} \tag{10}$$

corresponding, respectively, to the weakly unstable ion flute mode and the convective cells. In the absence of neutral beam injection, the thermal diffusion coefficient is generally small so that

$$\omega^*_n > k^2D \tag{11}$$

is satisfied for a small k. This means that the amplitude of the thermal convective cells in an inhomogeneous plasma is smaller than that in a homogeneous plasma since the energy in the flute mode dominates over the energy in the convective cells.[13] This does not necessarily mean the total diffusion is small in an inhomogeneous plasma since the ion flute mode is unstable.

In the presence of neutral beam injection, however, enhanced plasma convection and hence anomalous diffusion can take place so that it is possible to have

$$k^2 D \gtrsim \omega^*_n \tag{12}$$

in which the density gradient will not significantly reduce the diffusion due to plasma convective motion. For a given magnitude of diffusion coefficient which may be determined from the neutral beam injection, there is a critical density gradient given by $\omega^*_n = k^2 D$ beyond which the diffusion due to convective motion does not cause much diffusion since the ion flute mode dominates over the convective cells. This means that the steeper the density gradient, the smaller the plasma diffusion due to plasma convection. Note that the diffusion coefficient can be written as[6]

$$D = \frac{\langle(\Delta x)^2\rangle}{2\tau_c} = \frac{1}{2} V^2 \tau_c = \sum_k |V_k|^2 \frac{1}{2k^2 D} \quad , \tag{13}$$

where V_k is the random drift speed of a particle so that $D = [\sum_k |V_k|^2/2k^2]^{1/2}$. Since $\omega_n^* = k V_d^*$ where V_d^* is the ion diamagnetic drift speed, $k^2 D = \omega^*_n$ can be expressed as

$$V_d^* = k[\sum_k |V_k|^2/2k^2]^{1/2} \equiv |\bar{V}_k| \quad , \tag{14}$$

where $|\bar{V}_k|$ is the average random drift speed associated with the plasma convective motion defined by Equation (14) suggests that if the average convection speed is larger than the diamagnetic drift speed in the presence of neutral beam injection, then the presence of a density gradient will not

modify the diffusion due to convective motion of a plasma. Similar conclusions can be drawn on the different kind of drift motions of a plasma in a more complex magnetic field. In other words, when the viscosity damping k^2D is larger than the linear drift frequency, then the linear frequency is not important in determining the plasma diffusion due to plasma convection.

Similar convective motion is also generated in a plasma subject to localized heating across the magnetic field, such as due to RF heating of a plasma. Simulations show a presence of anomalous diffusion comparable to the diffusion of a plasma subject to neutral beam injection. Uniform plasma heating, such as due to alpha particles, does not generate any enhanced diffusion since no macroscopic convections appear in a plasma.

While the present simulations were carried out in a two-dimensional slab model in a uniform magnetic field, it is important to extend these calculations to three-dimensional linear and toroidal systems where the magnetic field is more complex.[5,12] While only the initial value simulations were carried out, it is possible to maintain a constant beam injection in time generating a steady-state anomalous diffusion. Results of such simulations will be reported elsewhere.

ACKNOWLEDGMENTS

This work was supported by the United States Department of Energy Contract No. DE-AC02-76-CHO-3073. In addition, one of the authors (HO) acknowledges support from the National Science Foundation grant ATM-85-12512.

REFERENCES

[1]L. A. Berry et al., in Proc. 5th International Conference of Plasma Physics and Controlled Nuclear Fusion, Tokyo, 1974, Vol. I, p. 113, IAEA (Vienna).

[2]H. Eubank et al., in Proc. 7th International Conference of Plasma Physics and Controlled Nuclear Fusion, Innsbruck, 1978, Vol. I, p. 167, IAEA (Vienna).

[3]F. H. Coensgen et al., in Proc. 6th International Conference of Plasma Physics and Controlled Nuclear Fusion, Berchtesgaden, 1976, Vol. III, p. 135, IAEA (Vienna).

[4]T. H. Stix, Plasma Phys. 14, 367 (1972).

[5]C. Z. Cheng and H. Okuda, Phys. Rev. Lett. 38, 708 (1977).

[6]H. Okuda and J. M. Dawson, Phys. Fluids 16, 408 (1973).

[7]H. Okuda, Phys. Fluids 23, 498 (1980).

[8]J. A. Byers and H. Grewal, Phys. Fluids, 13, 1819 (1970).

[9]J. R. Drake, J. R. Greenwood, G. A. Navratil, and R. S. Rost, Phys. Fluids 20, 148 (1977).

[10]G. A. Navratil, R. S. Rost, and A. B. Ekhardt, Phys. Fluids 20, 156 (1977).

[11]G. A. Navratil and R. S. Post, Comments Plasma Phys. Controlled Nucl. Fusion 5, 29 (1979).

[12]C. Z. Cheng and H. Okuda, Nucl. Fusion 18, 587 (1978).

[13]J. M. Dawson, H. Okuda, and B. Rosen, in Methods in Computational Physics, (Academic Press, New York, 1976), Vol. 16, p. 311.

FIGURE CAPTIONS

Fig. 1 Sketch of the simulation plasma model subject to perpendicular injection. A uniform density of beam particles localized in y with the width $\delta = L_y/4$ are injected into a uniform density ambient plasma perpendicular to magnetic field. Neutral particles are assumed to have ionized at $t = 0$ via various ionization processes in a plasma.

Fig. 2 Plots of the positions of the selected ions in the (x-y) plane at (a) $\omega_{pe}t = 0$, (b) 200, (c) 400 and (d) 800. Thermal plasma. Case 1.

Fig. 3 Plot of $\langle(\Delta y)^2\rangle$ with time. Spatial diffusion coefficient D_y is determined from the slope of the curve measured at a sufficiently long time. Case 1.

Fig. 4 Instantaneous contour plots of the electrostatic potential for a thermal plasma at (a) $\omega_{pe}t = 50$ and (b) $\omega_{pe}t = 500$. The amplitude of the contours varies from $e\phi/T = -0.87$ to $e\phi/T = 0.71$ for both (a) and (b). Case 1.

Fig. 5 Plots of the positions of the beam ions (a), (b) (upper panel) and the ambient ions (c), (d) (lower panel). (a) and (c) at $\omega_{pe}t = 250$; (b) and (d) at $\omega_{pe}t = 500$. Case 2.

Fig. 6 Plots of $\langle(\Delta x)^2\rangle$ for the beam ions and $\langle(\Delta y)^2\rangle$ for the ambient ions. $\omega_{ce} = 2\omega_{pe}$, $n_b = n_o/4$, and $V_o/V_i = 5$. Case 2.

Fig. 7 Total plasma density in y at $\omega_{pe}t = 0$ and 950. Note the dissipation of the initial density gradient generated by the neutral beam injection. Case 2.

Fig. 8 Total velocity distribution in v_x interpreted over v_y at $\omega_{pe}t$ = 5 and 500. Note the rapid thermalization of hot beam ions. Case 2.

Fig. 9 Time history of the ambient and beam ion average kinetic energy per particle normalized by the ambient thermal ion energy. Rapid initial relaxation is caused by the generation of a polarization electric field and loss-cone instability associated with the beam ions. Case 2.

Fig. 10 Plots of $\langle(\Delta x)^2\rangle$ for the beam ions and $\langle(\Delta y)^2\rangle$ for the ambient ions. $\omega_{ce} = 2\omega_{pe}$, $n_b = n_o$, and $V_o/V_i = 5$. Case 3.

Fig. 11 Instantaneous contour plots of the electrostatic potential for a plasma subject to neutral beam injection. Initial laminar structures shown in (a) at $\omega_{pe}t = 25$, gradually coalesce and become isotropic at later times at (b) $\omega_{pe}t = 125$, (c) $\omega_{pe}t = 250$, and (d) $\omega_{pe}t = 500$. The amplitude of the contours varies from $e\phi/T = -11$ to 11 for (a), $e\phi/T = -19$ to 19 for (b), $e\phi/T = -20$ to 21 for (c), and $e\phi/T = -22$ to 23 for (d). Case 3.

Fig. 12 Diffusion coefficient scaling with B. $n_b = n_o$ and $V_o/V_i = 5$ are fixed while $\omega_{ce}/\omega_{pe} = 1$, 2, and 4 are used.

Fig. 13 Plots of $\langle(\Delta x)^2\rangle$ for the beam ions and $\langle(\Delta y)^2\rangle$ for the ambient ions. $\omega_{ce} = 2\omega_{pe}$, $n_b = n_o$ and $V_o/V_i = 2.5$. Case 4.

Fig. 14 Plots of $\langle(\Delta x)^2\rangle$ and $\langle(\Delta y)^2\rangle$ for a plasma subject to localized heating in the central region with width $\delta = L_y/4$. $\omega_{ce} = \omega_{pe}$ and $T_h = 25T_c$. Case 5.

Fig. 15 Plots of the diffusion of the cold and hot ions uniformly distributed across a plasma column. $\omega_{ce} = \omega_{pe}$ and $T_h = 25T_c$. Hot ions have a Maxwellian velocity distribution. Case 6.

Fig. 16 Velocity space diffusion in a plasma where hot ions are initially monoenergetic. (a) Total ion velocity distribution in $f(v_x)$ integrated over v_y, at $\omega_{pe}t = 0$ and 500, and (b) $f(v_y)$ integrated over v_x at $\Omega_{pe}t = 0$ and 500. Case 7.

Fig. 17 Power spectrum of the mode $k = (2\pi/L_x, 2\pi/L_y)$ of the electric field in an arbitrary unit. Note the peaks near $\omega = \pm 3\ \omega_{ci}$ and $\omega = 0$. Case 7.

#86T0184

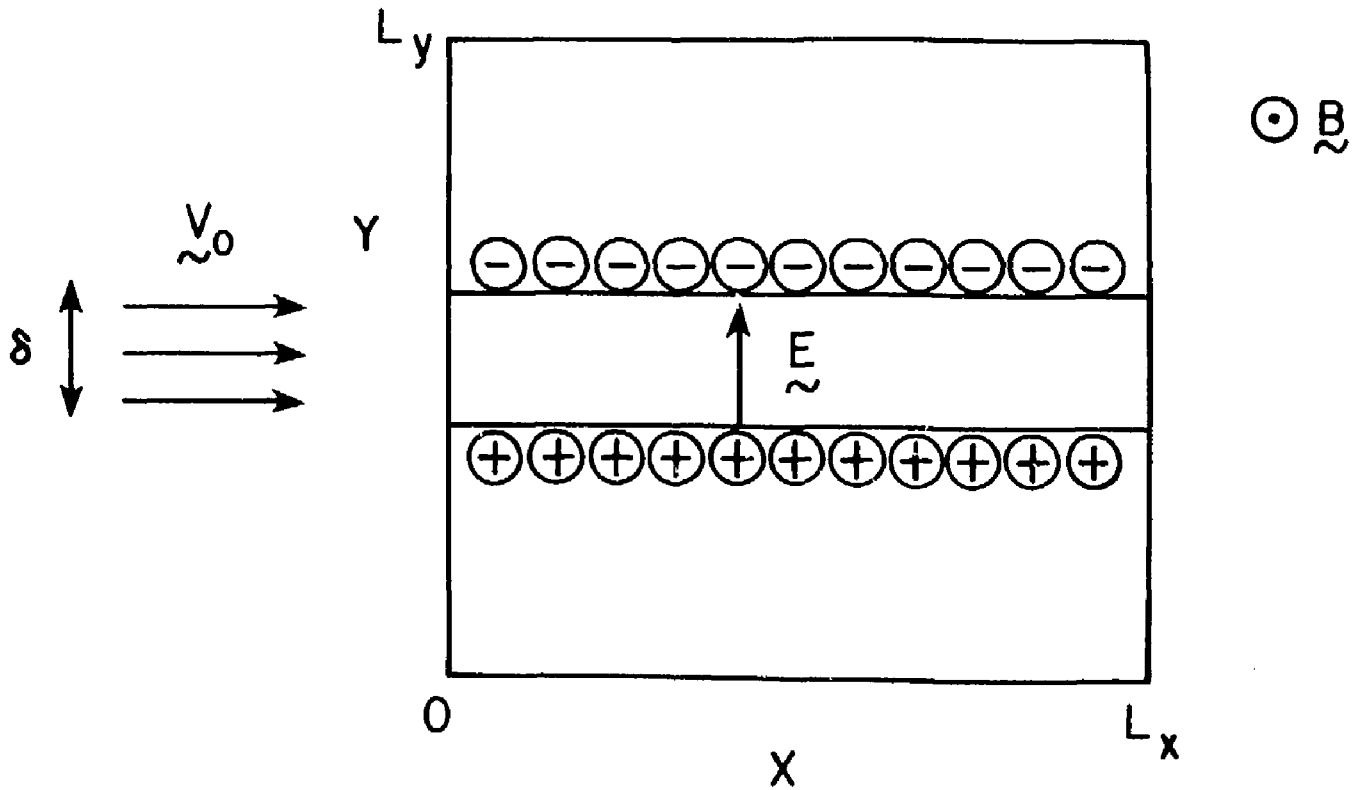

Fig. 1

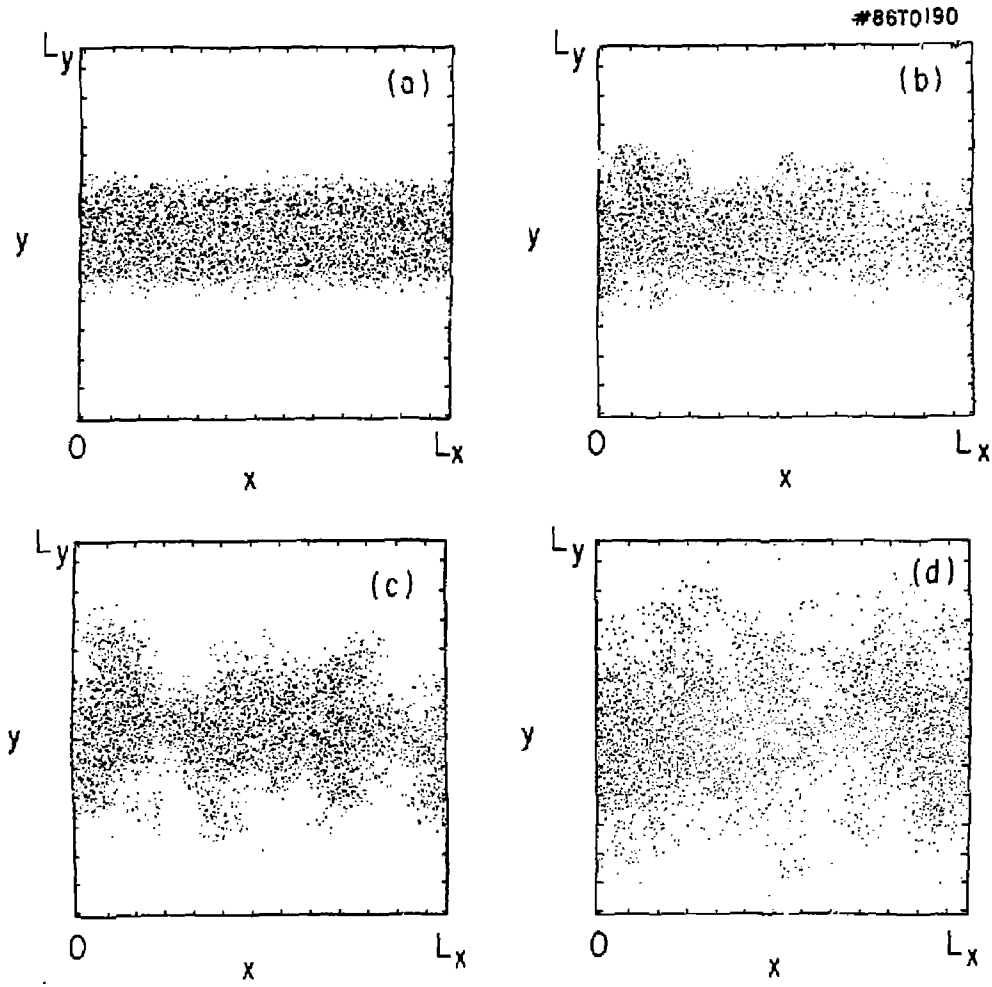

Fig. 2

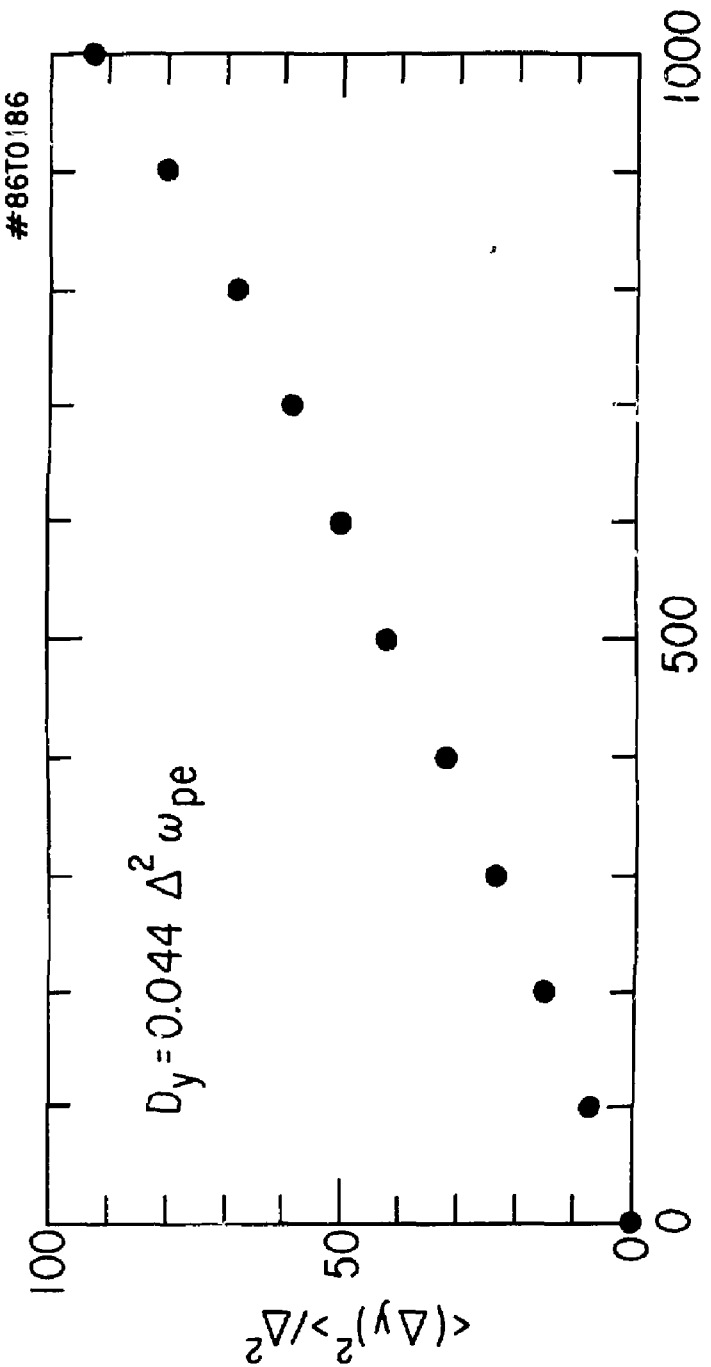
#86T0186
$D_y = 0.044\ \Delta^2 \omega_{pe}$
$\langle(\Delta y)^2\rangle/\Delta^2$
100
50
0
0
500
1000
$\omega_{pe}t$

Fig. 3

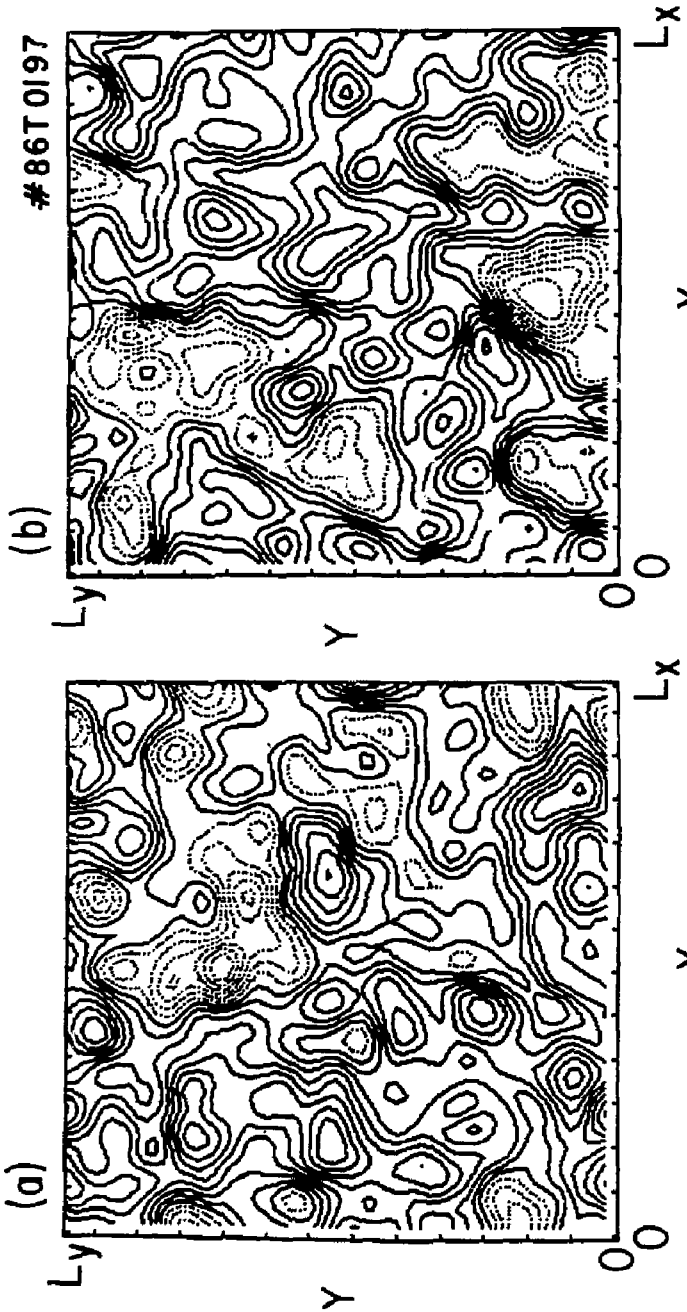

Fig. 4

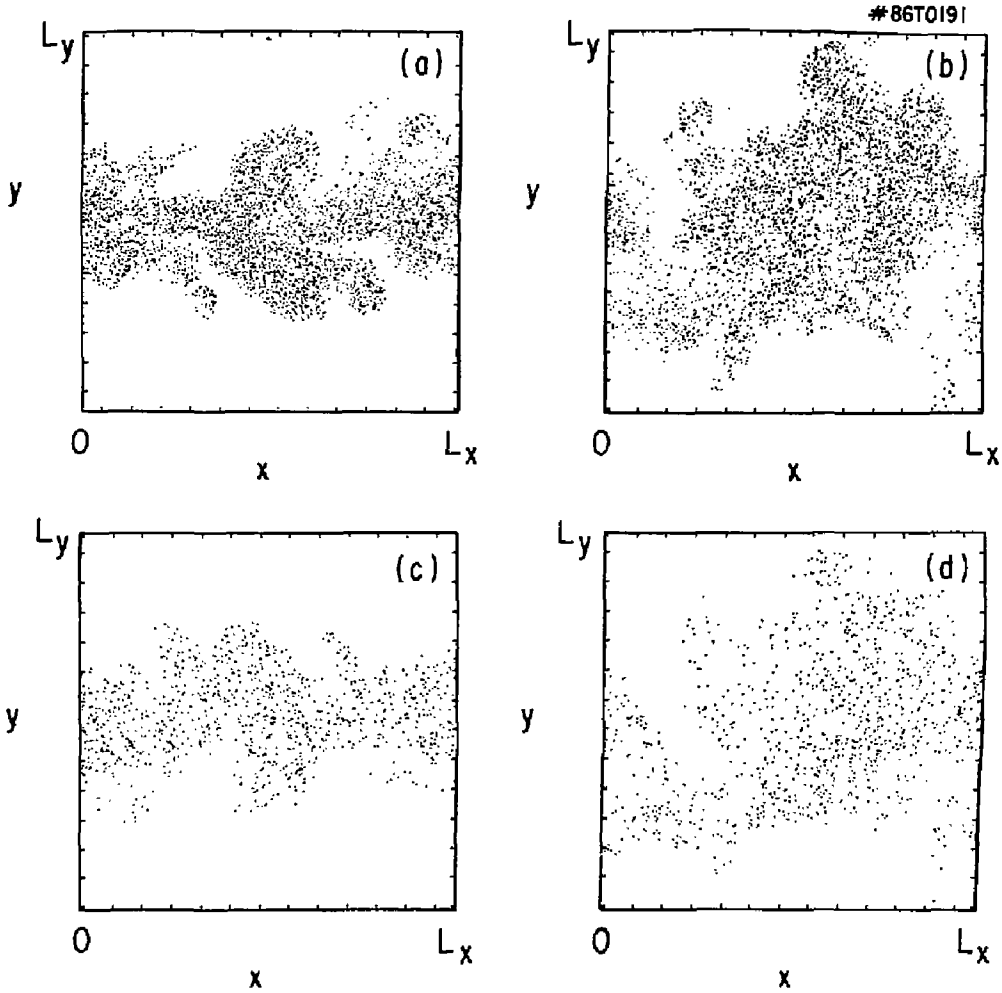

Fig. 5

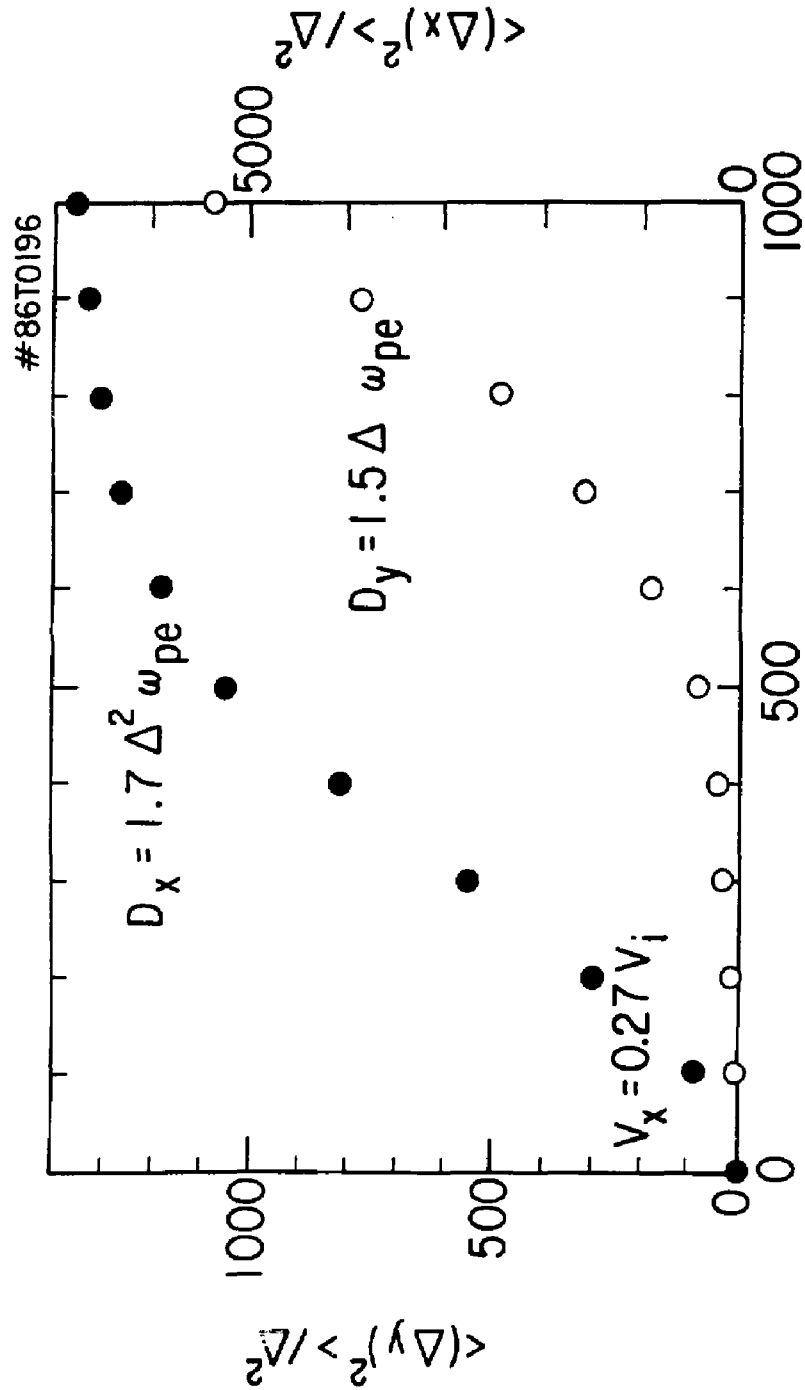
#86T0196
$<(\Delta y)^2>/\Delta^2$
$<(\Delta x)^2>/\Delta^2$
$D_x = 1.7\,\Delta^2\,\omega_{pe}$
$D_y = 1.5\,\Delta\,\omega_{pe}$
$V_x = 0.27\,V_i$
$\omega_{pe}t$
0
500
1000
5000

Fig. 6

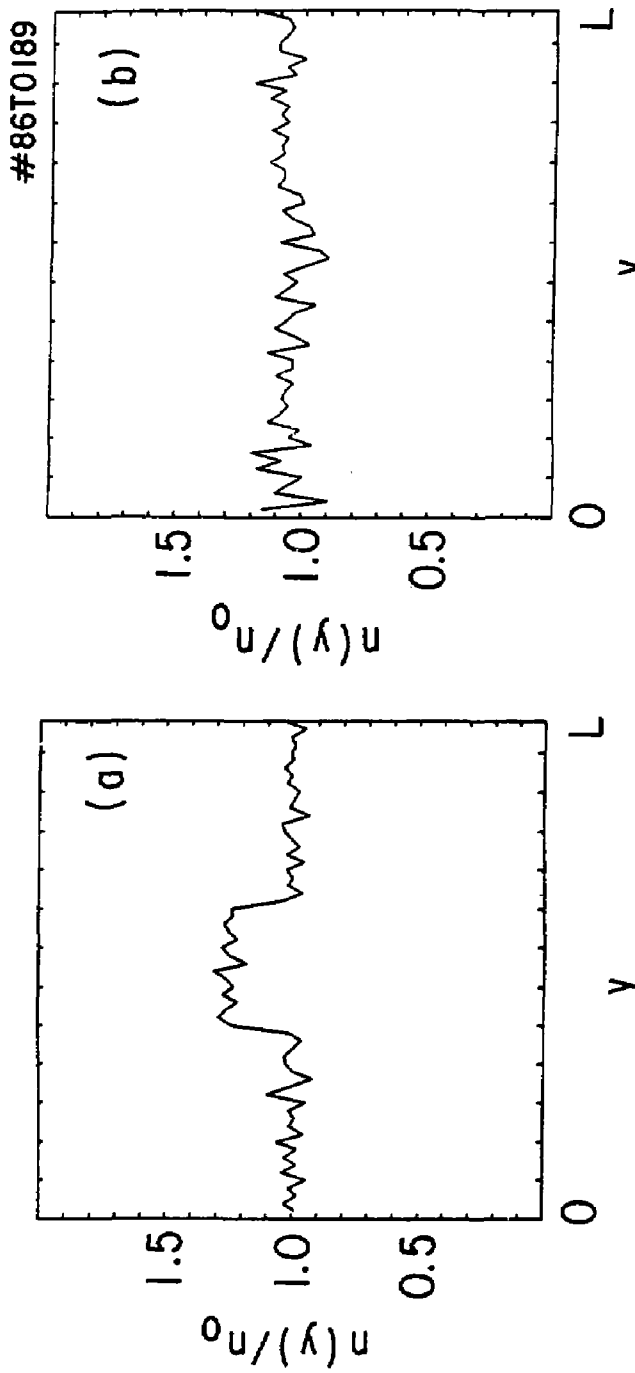

Fig. 7

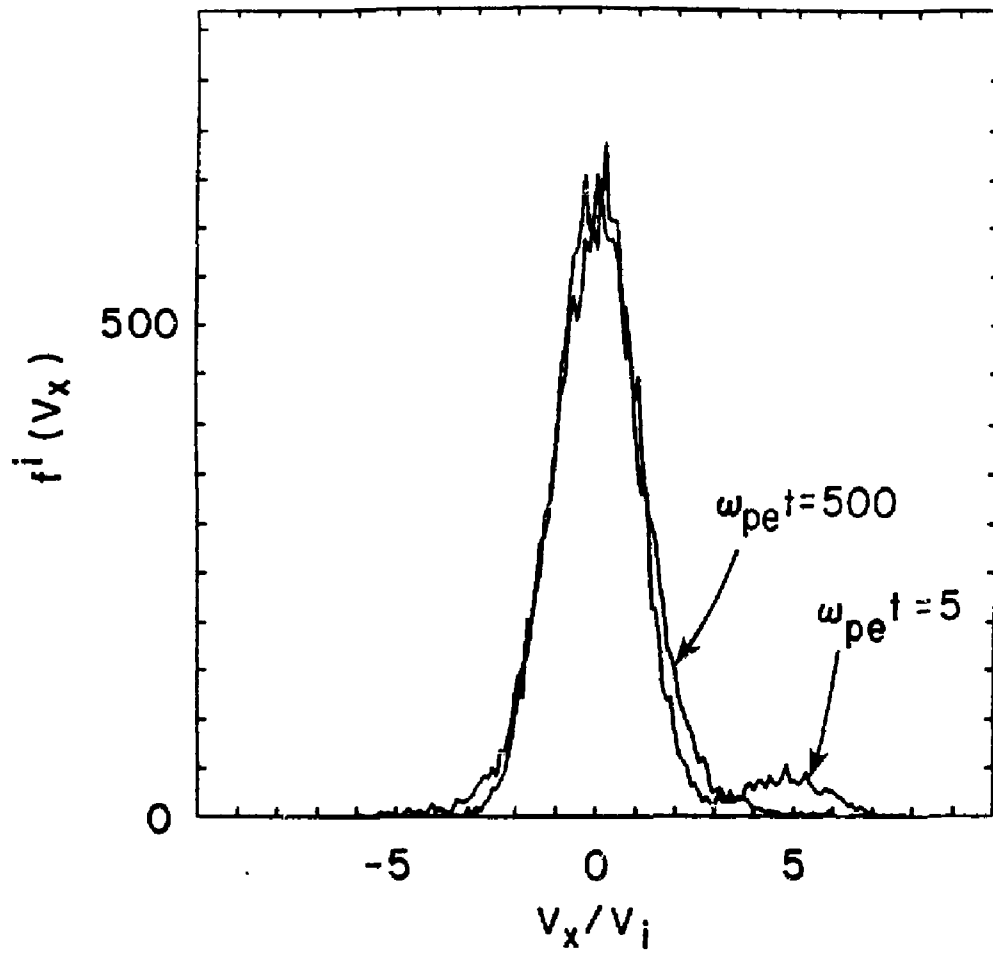

Fig. 8

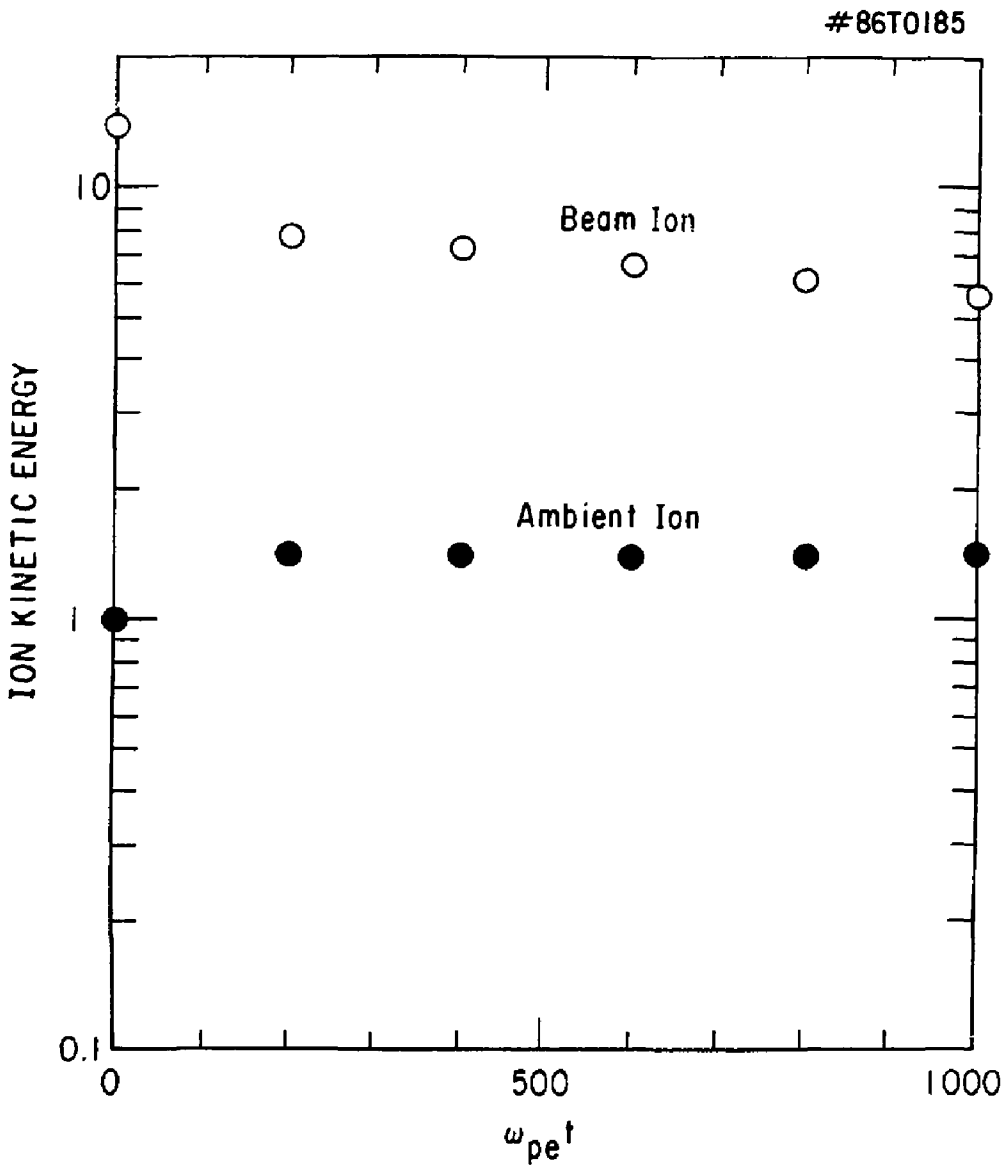
#86T0185
10
1
0.1
ION KINETIC ENERGY
Beam Ion
Ambient Ion
0
500
1000
$\omega_{pe}t$

Fig. 9

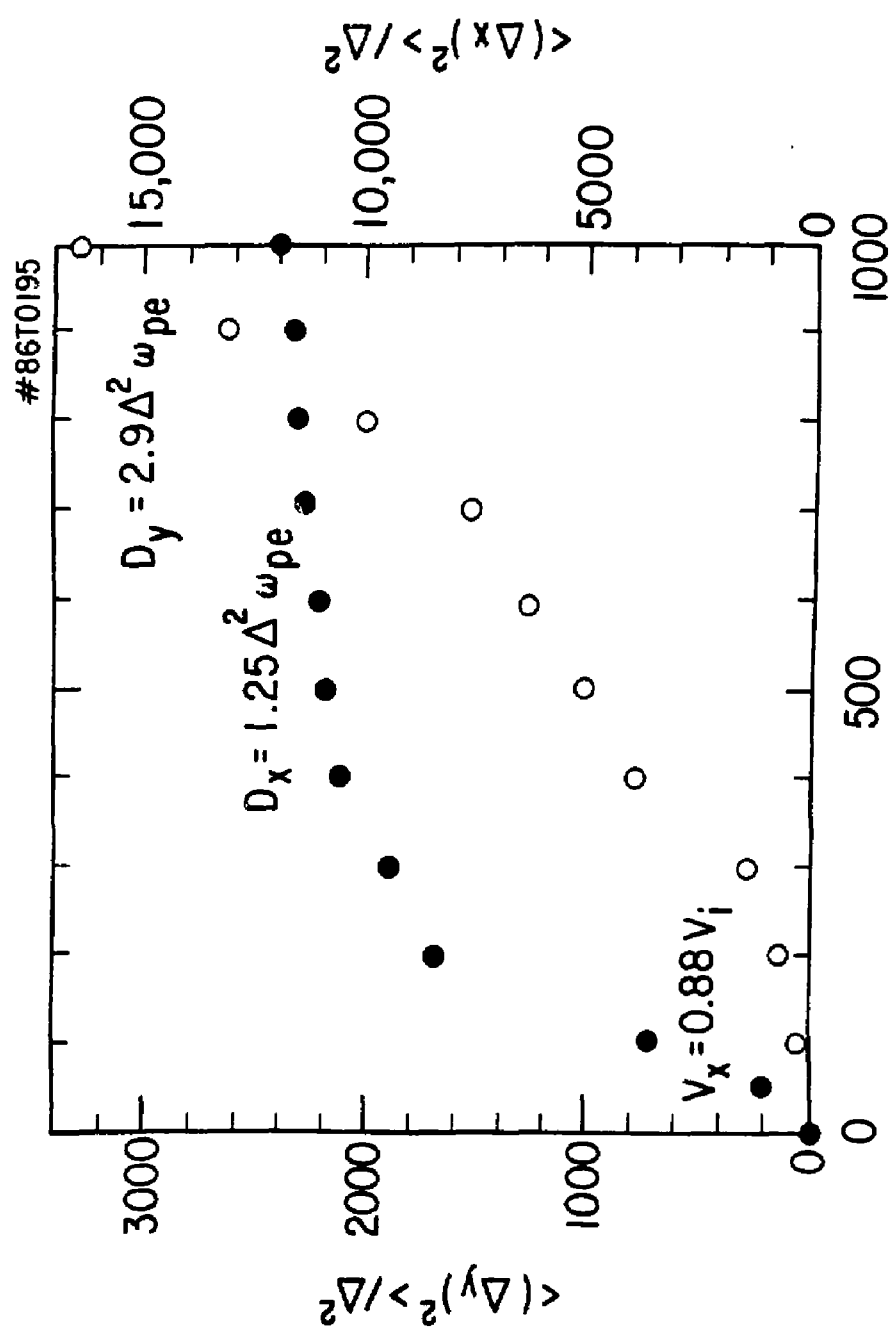
#86T0195
$D_y = 2.9\Delta^2\omega_{pe}$
$D_x = 1.25\Delta^2\omega_{pe}$
$V_x = 0.88 V_i$
$\omega_{pe}t$
$<(\Delta y)^2>/\Delta^2$
$<(\Delta x)^2>/\Delta^2$
0
500
1000
1000
2000
3000
5000
10,000
15,000

Fig. 10

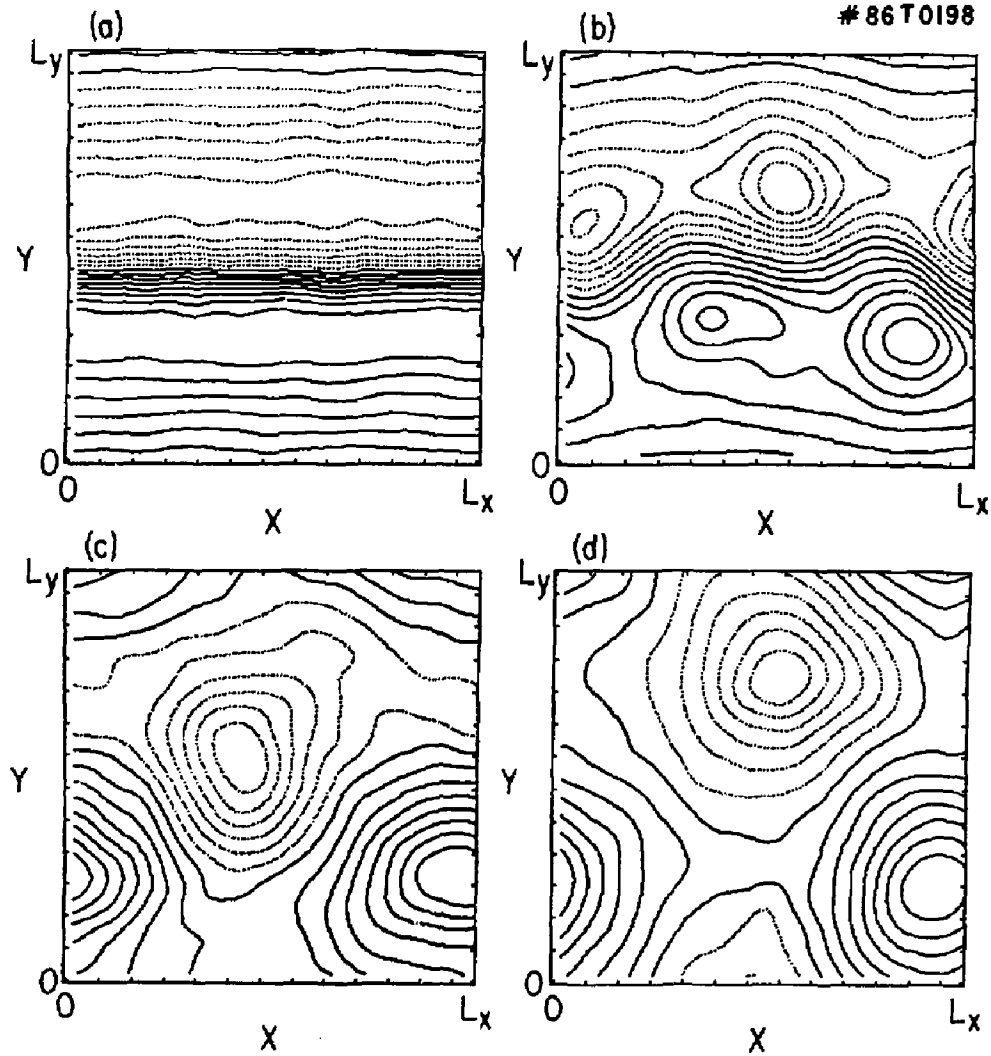

Fig. 11

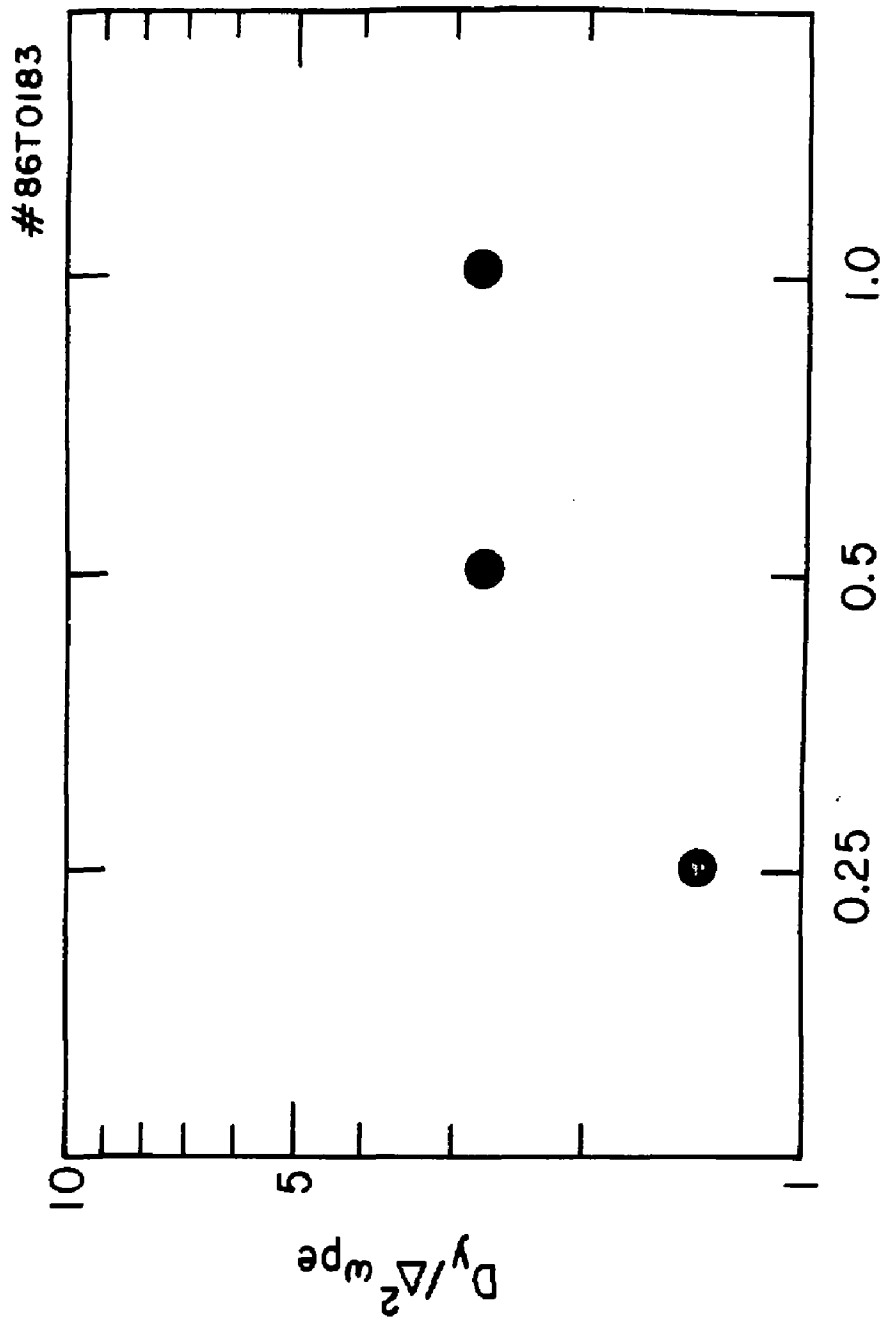

Fig. 12

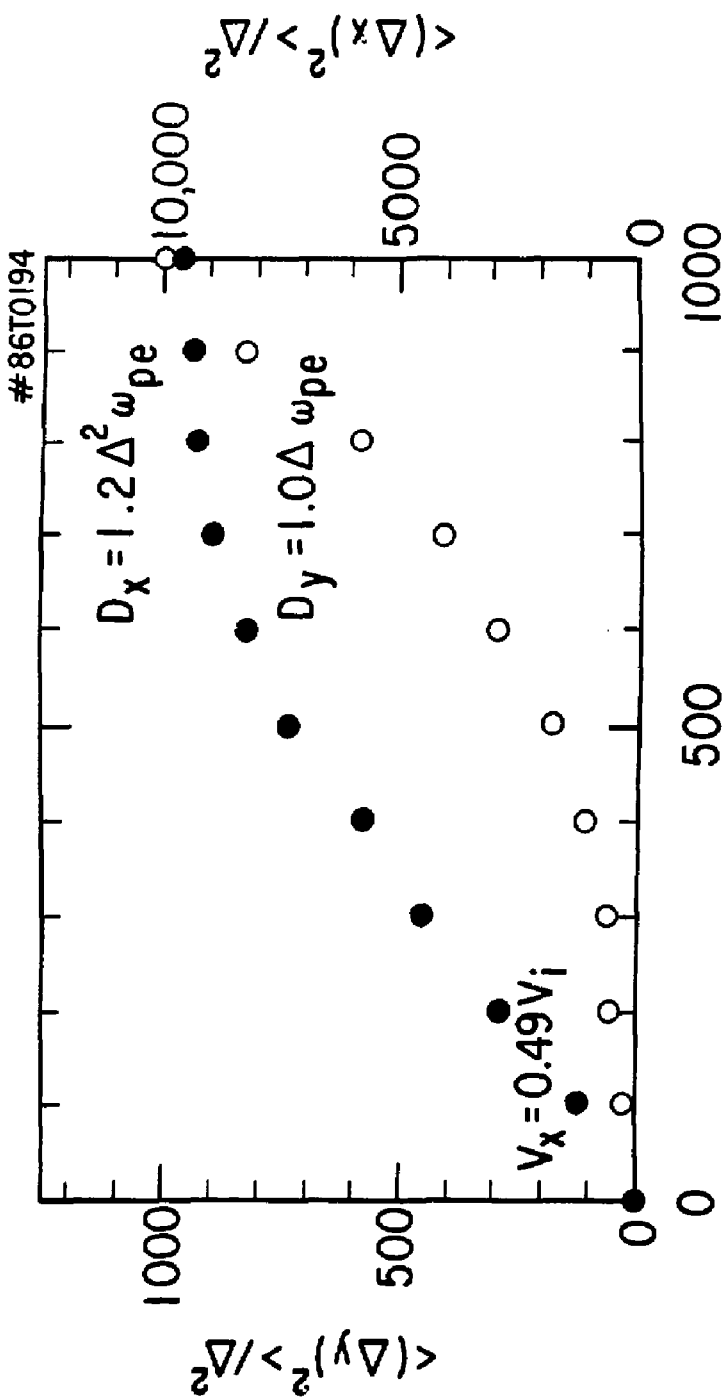
#86T0194
$D_x = 1.2\Delta^2\omega_{pe}$
$D_y = 1.0\Delta\,\omega_{pe}$
$V_x = 0.49V_i$
$\langle(\Delta y)^2\rangle/\Delta^2$
$\langle(\Delta x)^2\rangle/\Delta^2$
$\omega_{pe}t$
0
500
1000
5000
10,000

Fig. 13

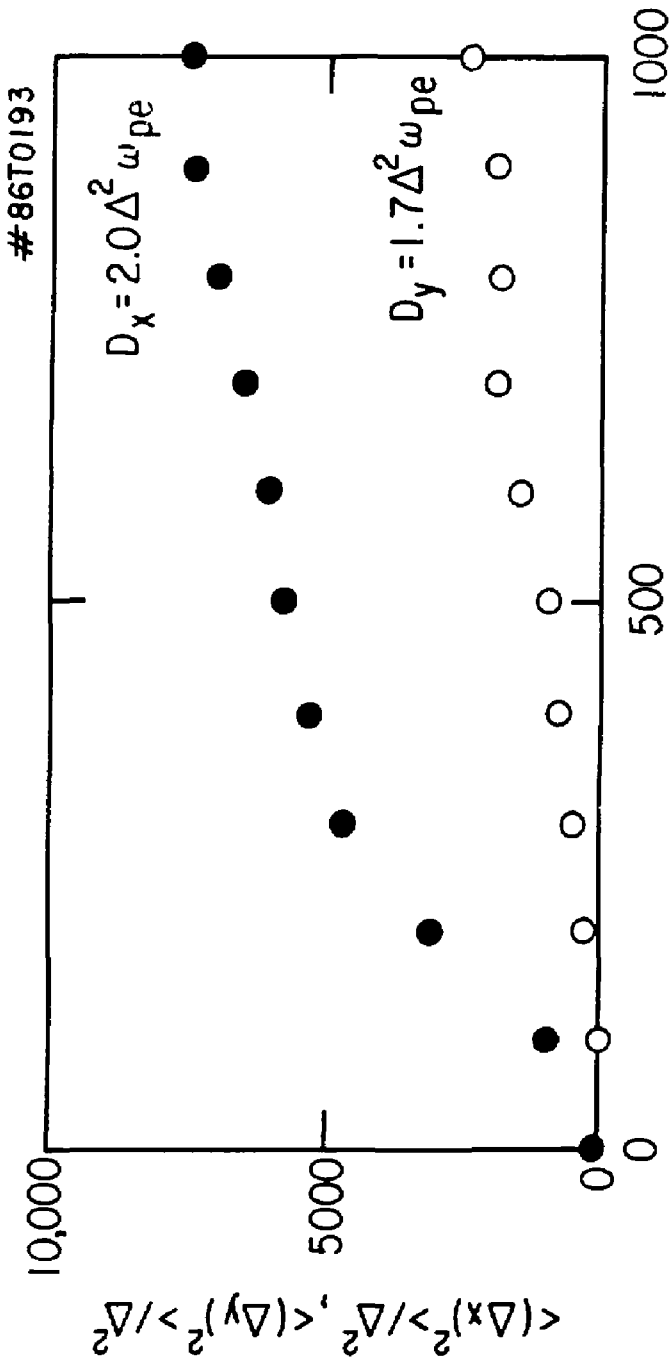
#86T0193
$D_x = 2.0\Delta^2\omega_{pe}$
$D_y = 1.7\Delta^2\omega_{pe}$
$\langle(\Delta x)^2\rangle/\Delta^2$, $\langle(\Delta y)^2\rangle/\Delta^2$
10,000
5000
0
0
500
1000
$\omega_{pe}t$

Fig. 14

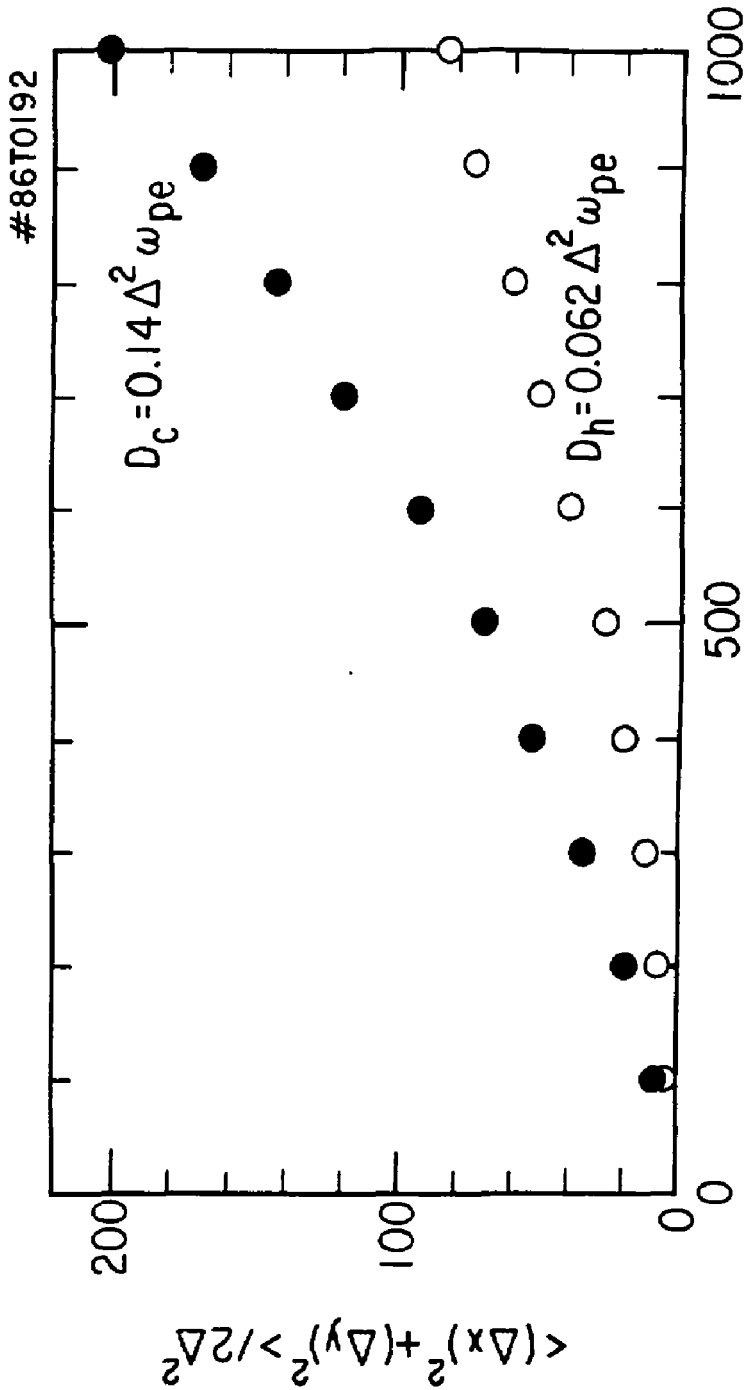
#86T0192
$D_c=0.14\Delta^2\omega_{pe}$
$D_h=0.062\Delta^2\omega_{pe}$
$<(\Delta x)^2+(\Delta y)^2>/2\Delta^2$
$\omega_{pe}t$
0
100
200
500
1000

Fig. 15

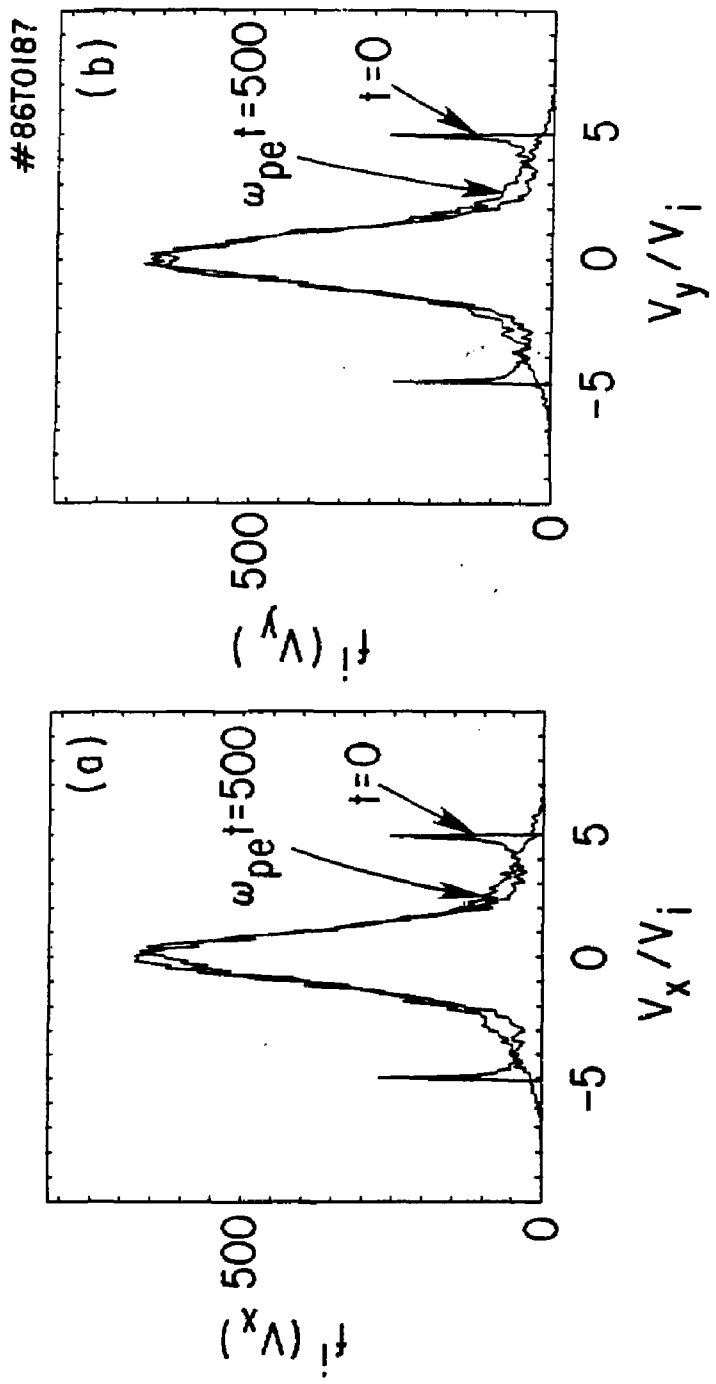

Fig. 16

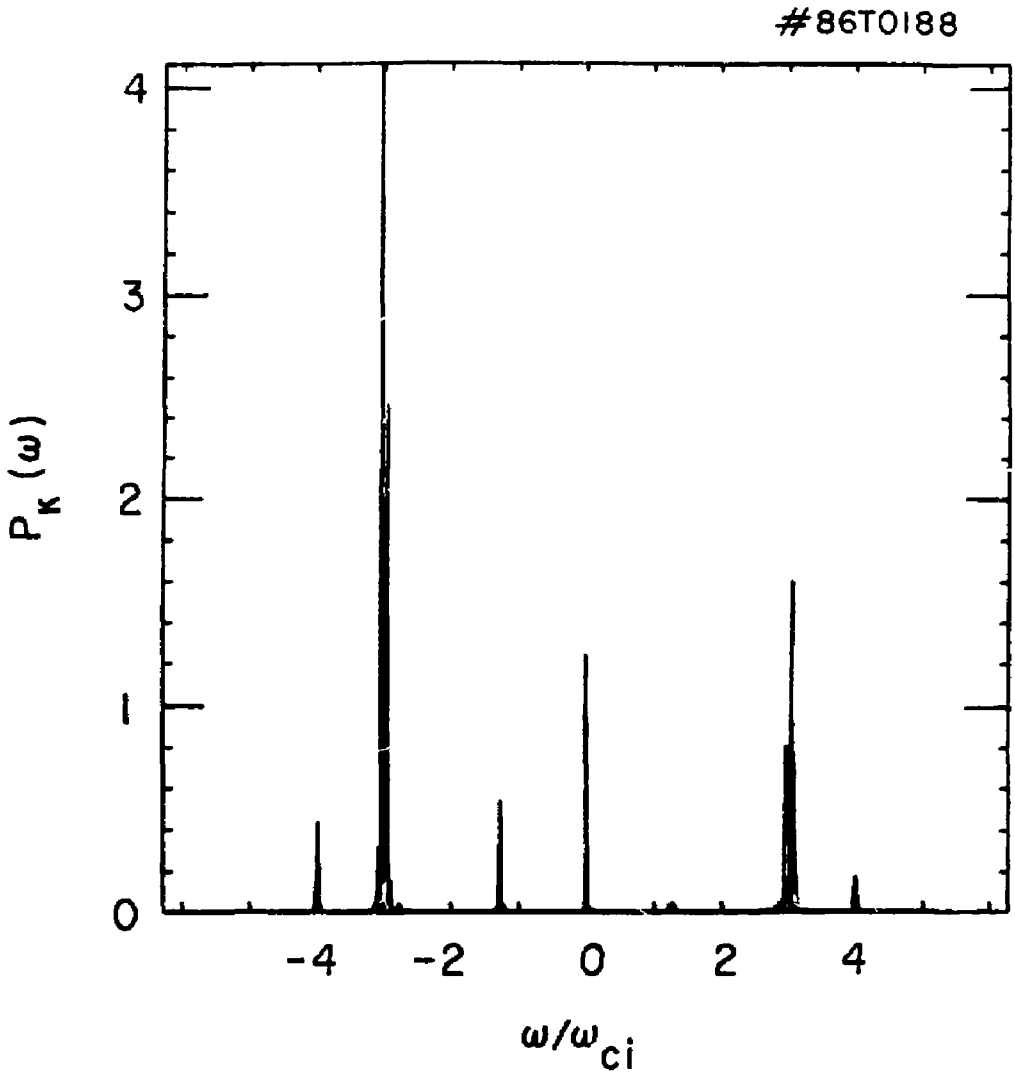

Fig. 17

EXTERNAL DISTRIBUTION IN ADDITION TO UC-20

Plasma Res Lab, Austra Nat'l Univ, AUSTRALIA
Dr. Frank J. Paoloni, Univ of Wollongong, AUSTRALIA
Prof. I.R. Jones, Flinders Univ., AUSTRALIA
Prof. M.H. Brennan, Univ Sydney, AUSTRALIA
Prof. F. Cap, Inst Theo Phys, AUSTRIA
M. Goossens, Astronomisch Instituut, BELGIUM
Prof. R. Boucique, Laboratorium voor Natuurkunde, BELGIUM
Dr. D. Palumbo, Dg XII Fusion Prog, BELGIUM
Ecole Royale Militaire, Lab de Phys Plasmas, BELGIUM
Dr. P.H. Sakanaka, Univ Estadual, BRAZIL
Lib. & Doc. Div., Instituto de Pesquisas Espaciais, BRAZIL
Dr. C.R. James, Univ of Alberta, CANADA
Prof. J. Teichmann, Univ of Montreal, CANADA
Dr. H.M. Skarsgard, Univ of Saskatchewan, CANADA
Prof. S.R. Sreenivasan, University of Calgary, CANADA
Prof. Tudor W. Johnston, INRS-Energie, CANADA
Dr. Hannes Barnard, Univ British Columbia, CANADA
Dr. M.P. Bachynski, MPB Technologies, Inc., CANADA
Chalk River, Nucl Lab, CANADA
Zhengwu Li, SW Inst Physics, CHINA
Library, Tsing Hua University, CHINA
Librarian, Institute of Physics, CHINA
Inst Plasma Phys, Academia Sinica, CHINA
Dr. Peter Lukac, Komenskeho Univ, CZECHOSLOVAKIA
The Librarian, Culham Laboratory, ENGLAND
Prof. Schatzman, Observatoire de Nice, FRANCE
J. Radet, CEN-BP6, FRANCE
JET Reading Room, JET Joint Undertaking, ENGLAND
AM Dupas Library, AM Dupas Library, FRANCE
Dr. Tom Mual, Academy Bibliographic, HONG KONG
Preprint Library, Cent Res Inst Phys, HUNGARY
Dr. R.K. Chhajlani, Vikram Univ, INDIA
Dr. B. Dasgupta, Saha Inst, INDIA
Dr. P. Kaw, Physical Research Lab, INDIA
Dr. Phillip Rosenau, Israel Inst Tech, ISRAEL
Prof. S. Cuperman, Tel Aviv University, ISRAEL
Prof. G. Rostagni, Univ Di Padova, ITALY
Librarian, Int'l Ctr Theo Phys, ITALY
Miss Clelia De Palo, Assoc EURATOM-ENEA, ITALY
Biblioteca, del CNR EURATOM, ITALY
Dr. H. Yamato, Toshiba Res & Dev, JAPAN
Direc. Dept. Lg. Tokamak Dev. JAERI, JAPAN
Prof. Nobuyuki Inoue, University of Tokyo, JAPAN
Research Info Center, Nagoya University, JAPAN
Prof. Kyoji Nishikawa, Univ of Hiroshima, JAPAN
Prof. Sigeru Mori, JAERI, JAPAN
Prof. S. Tanaka, Kyoto University, JAPAN
Library, Kyoto University, JAPAN
Prof. Ichiro Kawakami, Nihon Univ, JAPAN
Prof. Satoshi Itoh, Kyushu University, JAPAN
Dr. D.I. Choi, Adv. Inst Sci & Tech, KOREA
Tech Info Division, KAERI, KOREA
Bibliotheek, Fom-Inst Voor Plasma, NETHERLANDS
Prof. B.S. Liley, University of Waikato, NEW ZEALAND
Prof. J.A.C. Cabral, Inst Superior Tecn, PORTUGAL
Dr. Octavian Petrus, ALI CUZA University, ROMANIA
Prof. M.A. Hellberg, University of Natal, SO AFRICA
Dr. Johan de Villiers, Plasma Physics, Nucor, SO AFRICA
Fusion Div. Library, JEN, SPAIN
Prof. Hans Wilhelmson, Chalmers Univ Tech, SWEDEN
Dr. Lennart Stenflo, University of UMEA, SWEDEN
Library, Royal Inst Tech, SWEDEN
Centre de Recherchesen, Ecole Polytech Fed, SWITZERLAND
Dr. V.T. Tolok, Kharkov Phys Tech Ins, USSR
Dr. O.D. Ryutov, Siberian Acad Sci, USSR
Dr. G.A. Eliseev, Kurchatov Institute, USSR
Dr. V.A. Glukhikh, Inst Electro-Physical, USSR
Institute Gen. Physics, USSR
Prof. T.J.M. Boyd, Univ College N Wales, WALES
Dr. K. Schindler, Ruhr Universitat, W. GERMANY
ASDEX Reading Rm, IPP/Max-Planck-Institut fur Plasmaphysik, F.R.G.
Nuclear Res Estab, Julich Ltd, W. GERMANY
Librarian, Max-Planck Institut, W. GERMANY
Bibliothek, Inst Plasmaforschung, W. GERMANY
Prof. R.K. Janev, Inst Phys, YUGOSLAVIA